Hybrid multibend achromat lattice with sextupole cancellation across a straight section

Jiajie Tan, Jianhao Xu, Penghui Yang, Zhenghe Bai,* and Lin Wang†

National Synchrotron Radiation Laboratory, University of Science and Technology of China, Hefei 230029, China

(Received 6 December 2022; accepted 6 December 2023; published 27 December 2023)

The hybrid multibend achromat (HMBA) lattice concept is adopted in some diffraction-limited storage ring designs, which can permit relatively large on-momentum dynamic aperture and relatively weak sextupoles. In a typical HMBA lattice, the main arc section is constrained by the transverse phase advances making $-I$ transformation for sextupole cancellation. In this paper, a new HMBA lattice concept with sextupole cancellation across a straight section is proposed, where $-I$ is made between adjacent dispersion bumps of two lattice cells. This makes the main arc section free of the phase advance constraint, and as a result, the number of bending magnets (bends) in the lattice cell and the cell tunes can be easily changed, thus providing more choices for lattice design. To achieve the large phase advances required for $-I$ in this new concept, the split bend is used as the matching bend, which is a bend split into two pieces with a quadrupole in between. The split bend also serves to reduce the emittance, and the large phase advances also give low beta functions in the straight section enhancing the insertion device brightness. Besides, for a given emittance goal, this new HMBA lattice can have fewer bends than the typical HMBA lattice due to stronger focusing in bend unit cells, which is beneficial for saving space and suppressing intrabeam scattering effect. Two lattices are given as examples to demonstrate this new concept and show its linear and nonlinear properties and further extension is also discussed.

DOI: 10.1103/PhysRevAccelBeams.26.121602

I. INTRODUCTION

We can relate the natural emittance of an electron storage ring to several parameters as [1]

$$\varepsilon_x = FC_q \frac{E^2}{J_x N_b^3}, \tag{1}$$

where F is a ring lattice dependent factor, E is the electron energy, J_x is the horizontal damping partition number, and N_b is the number of bending magnets (bends) in the ring. Due to the inverse third-power dependence of ε_x on N_b, multibend achromat (MBA) lattices [2] are used for designing diffraction-limited storage rings (DLSRs). Among them, the hybrid MBA (HMBA) lattice concept [3,4], developed by ESRF-EBS, has been adopted in some DLSR designs for its relatively large on-momentum dynamic aperture (DA) and relatively weak sextupoles. This is attributed to the creation of a pair of dispersion bumps on both sides of the lattice arc section, separated by a $-I$ transformation with horizontal and vertical phase advances of $(3\pi, \pi)$, which can make a high efficiency of chromaticity correction and a very effective sextupole cancellation. However, the constraint of phase advances also limits the flexibility of the HMBA lattice. The number of bends in the lattice cell cannot be easily changed, and it is also difficult to reduce the lattice factor F.

Some variants of HMBA lattice have been proposed to pursue better performances and different requirements for DLSRs. The H7BA lattice of APS-U [5] introduced reverse bends (RBs) [6] to reduce the emittance; the H6BA lattices of DIAMOND-II [7] and HALF [8] have an additional straight section in the middle part, replacing the central bend to accommodate more insertion devices (IDs). In these lattices, the phase advances between two bumps for $-I$ remain unchanged. Though other phase advances can be chosen for $-I$, such as $(5\pi, \pi)$ for an H10BA lattice [9] and (π, π) for an H6BA lattice [10,11], this discontinuous choice with a horizontal interval of 2π restricts both the number of bends in the $-I$ part and the cell tunes to a large extent. A variable number of bends and adjustable cell tunes are beneficial for lattice design, which can, for example, reduce the emittance and better satisfy other needs.

Compared to some conventional MBA lattices [12–14], HMBA lattices need more total number of bends to reach

*baizhe@ustc.edu.cn
†wanglin@ustc.edu.cn

Published by the American Physical Society under the terms of the Creative Commons Attribution 4.0 International license. Further distribution of this work must maintain attribution to the author(s) and the published article's title, journal citation, and DOI.

the same emittance goal [15] due to relatively weak focusing in their bend unit cells (corresponding to relatively large lattice factor F), which will make weaker dipole fields and thus longer damping times. For example, the horizontal tune of the H7BA lattice cell is obviously smaller than that of the SLS-2 7BA lattice cell. Longer damping times can cause a more serious intrabeam scattering (IBS) effect. This has been reflected in recently designed medium-energy HMBA lattices with emittances of only tens of pm rad [16,17], where higher energies of 3.5–4.0 GeV are chosen and also damping wigglers (DWs) are employed to significantly enhance radiation damping for suppressing IBS-induced emittance increase and reducing emittance. Therefore, if the HMBA lattice factor F is reduced by increasing the focusing of bend unit cells, less bends can be needed for a given emittance goal, which is good for suppressing IBS and saving space. However, this is also limited by the phase advance constraint in the arc section.

Moving the phase advance constraint from the main arc section to both sides of the lattice cell would solve the problems above. In this paper, we propose a new HMBA lattice concept with sextupole cancellation across a straight section, in which $-I$ is made between adjacent bumps of two cells. Due to that, the main arc section is no longer constrained by the phase advances, it is easy to change the number of bends and the cell tunes. However, to realize this concept, we need to increase the phase advances of both sides of the cell to about $(3\pi, \pi)$ for making $-I$, which is too large in the normal magnet layout. Inspired by the studies in Refs. [10,18], we use the split bend as the matching bend to increase the phase advances, and also the beta functions in the straight section are lowered. The former can also reduce the emittance, and the latter enhances the ID brightness. Besides, the relatively strong focusing in the split bends can also make the focusing in other bends stronger due to the need for optics matching, thus reducing the lattice factor F.

The content of this paper is organized as follows: In Sec. II, we describe the new HMBA lattice concept, and then some related properties of the split bend cell employed in the concept are studied using a simplified lattice model. In Sec. III, two HMBA lattices are presented as examples to illustrate the lattice concept and also to show the lattice properties. In Sec. IV, a possible lattice extension based on the sextupole cancellation of the concept is discussed. Finally, we summarize the conclusion in Sec. IV.

II. LATTICE CONCEPT

The upper part of Fig. 1 shows the schematic of $-I$ transformation made between two dispersion bumps of the typical HMBA lattice cell. The number of bends in the lattice cell and the cell tunes are largely dependent on the inner part of the arc section, which is, however, constrained by the phase advances for $-I$. To have better flexibility, here we propose a new HMBA lattice concept with sextupole cancellation across a straight section. As shown

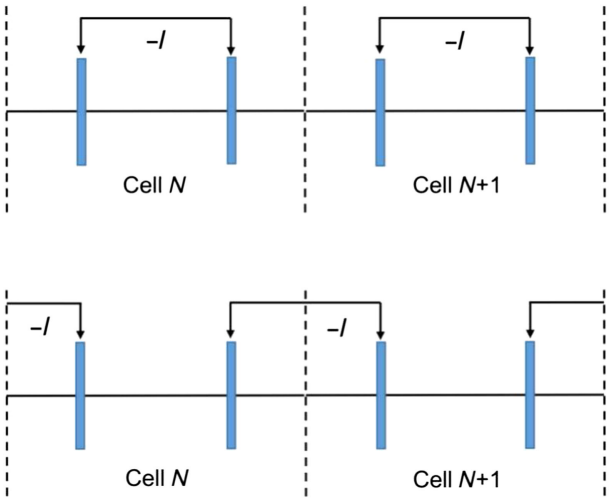

FIG. 1. Schematic of $-I$ transformation between two dispersion bumps for the typical HMBA lattice (upper) and new HMBA lattice (lower). The dashed vertical lines indicate the centers of straight sections.

in the lower part of Fig. 1, $-I$ is made between adjacent dispersion bumps of two lattice cells, which will make the inner part of the arc section free of the phase advance constraint. To do so, we need to get $-I$ with the matching sections and straight section, which is however difficult to realize with a normal magnet layout. In most HMBA lattice designs [3,4,7,8], the horizontal and vertical phase advances of the matching sections and straight section, denoted as $(\Delta\phi_x, \Delta\phi_y)$, are about $(0.9 \times 2\pi, 0.35 \times 2\pi)$, which are far from the required $(1.5 \times 2\pi, 0.5 \times 2\pi)$, especially in the horizontal plane. SOLEIL designed an HMBA lattice [19] with a very small horizontal beta function in the straight section, which has a larger $\Delta\phi_x$ of about $1.2 \times 2\pi$. However, it is still not enough to satisfy the required value for $-I$.

Inspired by the studies in [10,18], we introduce split bends as the matching bends so as to increase the phase advances $(\Delta\phi_x, \Delta\phi_y)$. The split bend is such a bend that is split into two pieces with a quadrupole in between. It increases phase advances by introducing additional focusing. We first use a simplified unit cell model shown in Fig. 2 to study the focusing property of split bend. A similar

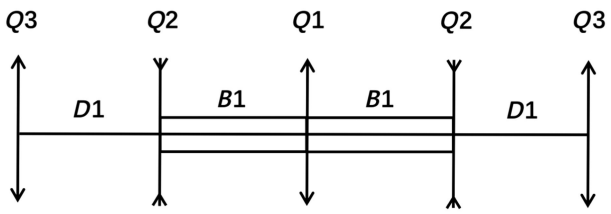

FIG. 2. Layout of the simplified unit cell model with split bend. In the model, $Q1$ and $Q3$ are horizontally focusing quadrupoles and $Q2$ is defocusing quadrupole; $D1$ is drift and $B1$ is half of the split bend.

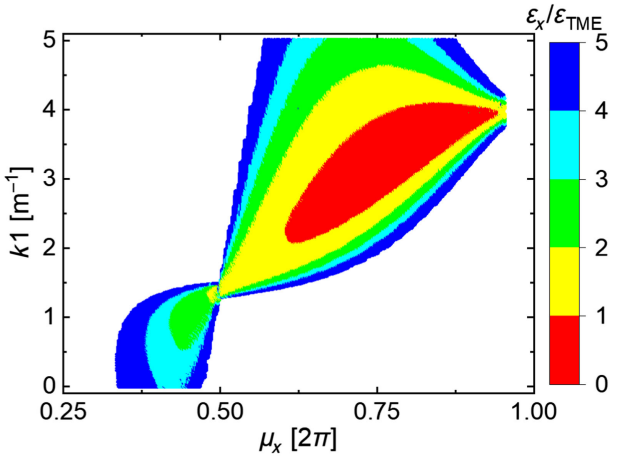

FIG. 3. Cell horizontal phase advance μ_x vs quadrupole strength $k1$ for scanned solutions, with color denoting the emittance ratio $\varepsilon_x/\varepsilon_{\mathrm{TME}}$.

cell model has been mentioned in Ref. [18], where the split bend cell was studied with fixed phase advances. Thin lens approximation is used for quadrupoles in this model. In the study, for simplicity, the ratio of the bend length to the total drift length is set to 1. Here we set the length of drift $D1$ to 1 m; half of the split bend, $B1$, has a length of 1 m and a bending angle $\theta/2$ of 1°. The whole ring consists of 180 identical cells. The strengths $k1$, $k2$, and $k3$ of three quadrupole families $Q1$, $Q2$, and $Q3$ are allowed to vary in the ranges of $[0, 5]$, $[-5, 0]$, and $[0, 5]$ m^{-1}, respectively. We scanned the quadrupole strengths with the step of 0.01 m^{-1}.

Figure 3 presents the results of scanned solutions. The emittances of solutions are compared to the theoretical minimum emittance (TME) [20], $\varepsilon_{\mathrm{TME}}$, with the same bending angle θ, which are shown as ratios of $\varepsilon_x/\varepsilon_{\mathrm{TME}}$ in the figure. The solutions with emittances larger than $5 \times \varepsilon_{\mathrm{TME}}$ are not shown in the figure. The split bend cell becomes a TME-like cell when $k1 = 0$. When $k1$ has a small value, the horizontal phase advance of the unit cell, μ_x, is less than $0.5 \times 2\pi$. As $k1$ increases, μ_x shifts its maximum toward 2π and lower emittance can be obtained. This means that we can get a horizontal phase advance of $1.5 \times 2\pi$ with two split bend unit cells. The red area indicates that the emittance can be reduced to lower than $\varepsilon_{\mathrm{TME}}$ with appropriate values of $k1$ and μ_x, since in this case the split bend cell can be seen as a combination of two TME-like cells, each with a bending angle of $\theta/2$.

Our goal is to make an HMBA lattice with $-I$ across a straight section by employing split bends. The $-I$ part of this HMBA lattice can be seen as a double-bend achromat (DBA) lattice cell with two split bends, which has horizontal and vertical phase advances of about $(3\pi, \pi)$. Then we study the DBA cell with split bends using a simplified model similar to the unit cell model above. As shown at the top of Fig. 5, the layout from the first quadrupole to the center of the DBA cell is like the model in Fig. 2. The difference is that the parameters and positions of magnets are not symmetric about the quadrupole inserted in the split bend (hereafter called split-bend quadrupole). In the DBA cell model, the sum of bending angles of two pieces of the split bend is also set to $\theta = 2°$ and the sum of their lengths is 2 m, and the sum of two different drifts between quadrupoles is 2 m (i.e., here the ratio of the bend length to the total length of two drifts is also 1). Besides, the length of the straight section is set to 5 m. With these settings, the NSGA-III algorithm [21] was used to study the DBA cell, with magnet parameters and positions as variables.

In the study, the optimization objectives are to minimize the split-bend quadrupole strength $k1$ and the emittance ratio $\varepsilon_x/\varepsilon_{\mathrm{DBA}}$, where $\varepsilon_{\mathrm{DBA}}$ is the minimum emittance of DBA lattice, with $\varepsilon_{\mathrm{DBA}} = 3 \times \varepsilon_{\mathrm{TME}}$ [22]. For the constraints, initially, we only considered the dispersion-free condition: the absolute dispersion in the straight section is less than 0.001 m. The optimized Pareto front of the two objectives is shown in the left plot of Fig. 4, and the horizontal phase advance of the DBA cell is also calculated and shown in the figure for these Pareto solutions. We see that as $k1$ increases, the minimum emittance obtained decreases roughly linearly, and the cell horizontal phase advance increases. When $k1 = 0$, i.e., the usual bend is used, the emittance is about $1.5 \times \varepsilon_{\mathrm{DBA}}$.

Then, the cell phase advance condition was further considered as the second constraint in the study. For this constraint, we set the horizontal phase advance in the range of 1.48–$1.52 \times 2\pi$ and the vertical in the range of 0.48–$0.52 \times 2\pi$. Note that the horizontal and vertical phase advances cannot be exactly equal to 3π and π, respectively, for having a stable solution. Due to that the dispersion-free and phase advance constraints we set here are very stringent, it is very difficult to obtain the true Pareto front for the two objectives [23]. So we scanned $k1$ so as to obtain better results, and at each value of $k1$, $\varepsilon_x/\varepsilon_{\mathrm{DBA}}$ was minimized. The optimization results are shown in the right plot of Fig. 4, and for these solutions, their horizontal beta functions at the center of the straight section, $\beta_{x,0}$, are also shown as additional information. We see that with the phase advance constraint further considered, the emittance also decreases roughly linearly with increasing $k1$ and the minimum emittance is slightly less than $0.5 \times \varepsilon_{\mathrm{DBA}}$. We also see that as $k1$ increases, $\beta_{x,0}$ increases but is less than 3 m. The optimum beta function for matching the electron and photon beam phase spaces to enhance the ID brightness is $\beta_{x,0} = L/\pi$ [24] with L being the ID length. It is interesting to see that at smaller $k1$, the emittance is larger and $\beta_{x,0}$ is too small (less than 1 m), both of which are not good for brightness enhancement. While at larger $k1$, both lower emittance and reasonably low $\beta_{x,0}$ can promise higher brightness.

Such a DBA lattice cell with phase advances of about $(3\pi, \pi)$ is shown in Fig. 5. The emittance of this DBA lattice

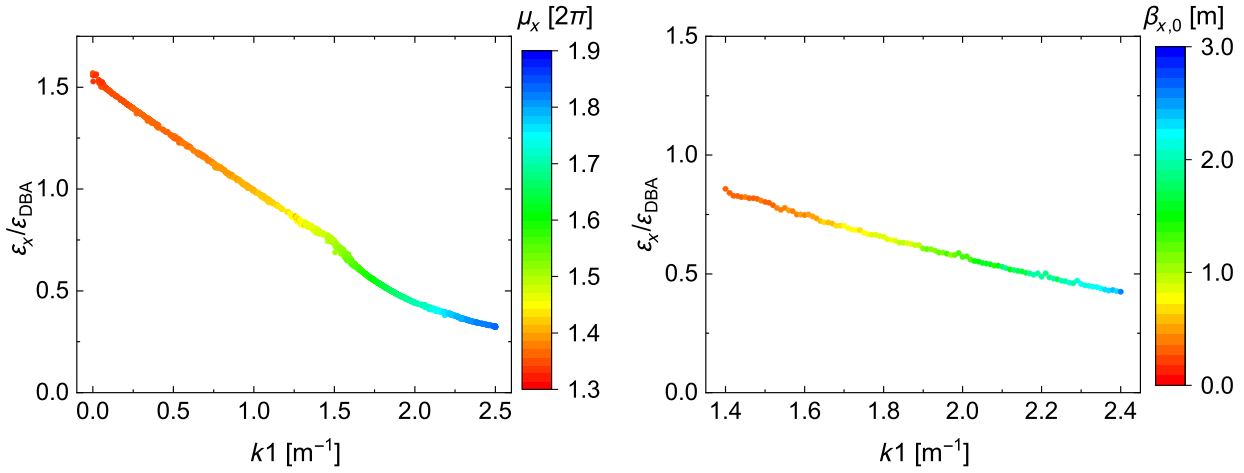

FIG. 4. Left: Pareto front of split-bend quadrupole strength $k1$ and emittance ratio $\varepsilon_x/\varepsilon_{\mathrm{DBA}}$ for a DBA cell model, where the color denotes the cell horizontal phase advance. Right: $k1$ vs minimum $\varepsilon_x/\varepsilon_{\mathrm{DBA}}$ for the DBA cell model with phase advances of about $(3\pi, \pi)$, where the color denotes the horizontal beta function at the center of the straight section.

is $0.64 \times \varepsilon_{\mathrm{DBA}}$. The split bend of this DBA lattice is not divided into two identical pieces as that of the unit cell shown in Fig. 2. The outer piece at lower dispersion has a shorter length and higher dipole field compared to the inner piece. As the same principle of longitudinal gradient bend (LGB) [25,26] for reducing the emittance, distributing a high dipole field at the position with low dispersion can help to suppress the quantum excitation, thus giving small dispersion action $\mathcal{H}_x$. Besides, the horizontal and vertical beta functions in the straight section have small values so that the ID brightness can be further enhanced.

In addition, the focusing in the split bend of this DBA lattice is relatively strong. When other bends are inserted in the middle part to make the new HMBA lattice, the focusing on these bends can also become strong due to the need for better optics matching, which will be shown in the practical lattice design of the next section.

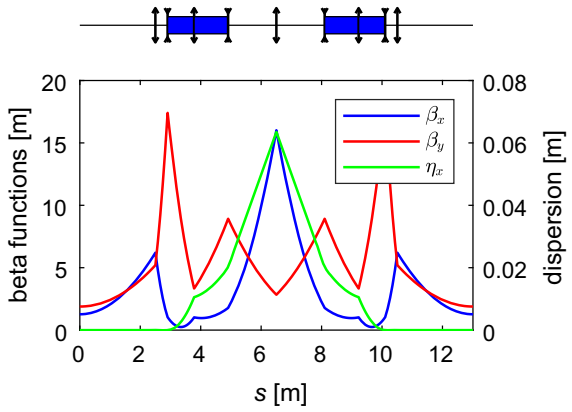

FIG. 5. Simplified model layout and optical functions of a DBA lattice cell with split bends, which has horizontal and vertical phase advances of about $(3\pi, \pi)$. In the layout, split bends are shown in blue, and thin-lens quadrupoles are shown as arrows.

III. EXAMPLES

As examples, an H8BA lattice and an H6BA lattice with sextupole cancellation across a straight section were preliminarily designed. To be consistent with the naming of an HmBA lattice with split bends in Ref. [10], in this section, the split bend is regarded as two bends. The two designs have the same energy of 3 GeV and the same storage ring circumference of 460.8 m. The H8BA design has 20 lattice cells, and the H6BA design has 24 cells. The NSGA-III algorithm was also used in the lattice design. Following Ref. [9], in the linear optics optimization, not only the natural emittance but also the natural chromaticities and integrated strengths of sextupoles were optimized so that the lattice solutions with potentially good nonlinear dynamics can be realized.

A. H8BA lattice

Figure 6 shows the magnet layout and linear optics of the designed H8BA lattice cell. Due to that the matching bend, i.e., the split bend, has two pieces of bends, this lattice is regarded as an H8BA lattice. In this lattice cell, the horizontal and vertical phase advances between the starting position and the peak of the first dispersion bump are about half of $(3\pi, \pi)$. Except that the two central bends are combined-function bends, the other main bends are LGBs, and two families of RBs are also employed to help reduce the natural emittance down to 74.5 pm rad. The main storage ring parameters of this design are listed in Table I, and the strengths of magnets (except LGBs) are shown in Table II. The beta functions at the center of the straight section have values of 1.5–3 m. Such small beta functions and ultralow emittance can significantly increase the ID brightness.

This H8BA lattice can be compared with the recent H9BA lattice of SSRL-X [16], which also uses split bends

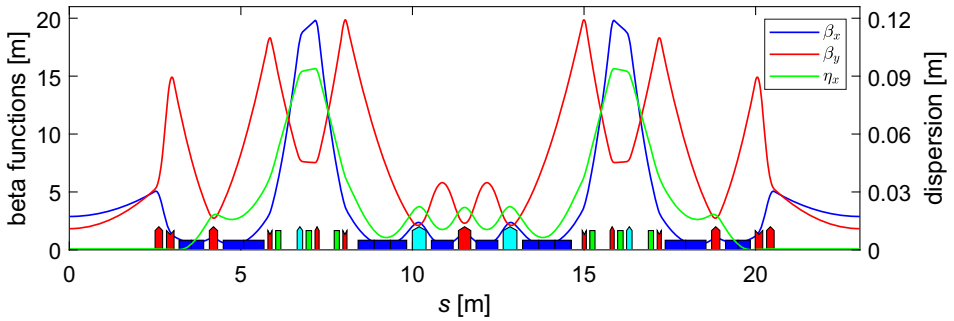

FIG. 6. Magnet layout and optical functions of the H8BA lattice cell. Main bends are in blue, RBs in cyan, quadrupoles in red, and sextupoles in green.

and has low beta functions in the straight section. However, the main arc section of the H9BA lattice is constrained by $-I$. The horizontal tune of the H9BA lattice cell is about 2.76, while the H8BA lattice cell has a larger horizontal tune of about 2.81, though it has a smaller number of bends. This means that the bend unit cells of the H8BA lattice have stronger focusing. For an emittance goal, a smaller number of bends together with stronger focusing will generally give higher dipole fields and thus shorter damping times, which is beneficial for suppressing the IBS induced emittance increase. A comparison between the H8BA and H9BA lattices was made and is shown in Table III, where the H9BA design is scaled to the same energy and number of cells as those of the H8BA design according to Eq. (1). We see that compared to the H9BA design, the H8BA design has lower emittance even though its J_x is smaller. Due to having fewer bends, the H8BA lattice can also save space compared to the H9BA lattice.

In the H8BA lattice, three families of sextupoles were used for the nonlinear optimization with the horizontal and vertical chromaticities corrected to (2, 2). Figure 7 shows the optimized on-momentum DA, tracked with ELEGANT [28]. We see that the horizontal 4D DA is about −8 to 6 mm, which is relatively large considering the ultralow emittance and the small horizontal beta function. With the rf cavity included, the DA shrinks due to the path lengthening effect as in other HMBA lattices. For simplicity, random magnet errors were considered based on the residual effects, such as a few percent beta beat, where there is no correction; and multipole field errors were also added. With these errors further included, the horizontal DA becomes about 3 mm.

Due to the $-I$ made across the straight section, the sextupole resonance driving terms [29] are not canceled

TABLE I. Main storage ring parameters of the H8BA and H6BA lattices.

Parameters	H8BA	H6BA
Energy (GeV)	3	
Circumference (m)	460.8	
Number of cells	20	24
Length of the straight section (m)		
Natural emittance (pm rad)	74.5	136.2
Betatron tunes (H/V)	56.14/15.18	52.21/17.13
Natural chromaticities (H/V)	−106.6/ − 100.0	−94.3/ − 88.9
Momentum compaction	1.29×10^{-4}	1.47×10^{-4}
Damping partition numbers (H/V/L)	1.91/1.0/1.09	1.58/1.0/1.41
Natural damping times (H/V/L) (ms)	13.8/26.3/24.0	14.3/22.6/16.0
Energy lost per turn (keV)	351.7	407.8
Natural energy spread	0.746×10^{-3}	0.717×10^{-3}
Total absolute bending angle (°)	410.4	406.7
β_x/β_y at the center of the straight section (m)	2.88/1.83	2.48/2.39
rf voltage[a] (MV) (w/o ID)	1.68	1.93
Touschek lifetime[b] (h)	2.1	3.1

[a]The rf momentum acceptance is set to 5%, and the rf frequency is 500 MHz.

[b]The bunch lengthening and magnet errors are not considered, and a 10%-coupling beam with bunch charge of 1 nC is assumed, which corresponds to a beam current of 400 mA with 80% buckets equally filled.

TABLE II. Magnet strengths of the H8BA and H6BA lattices. Here the LGB fields are not shown, and the definitions of sextupole and octupole strengths are 2 and 6 times, respectively, the definitions in the OPA code [27].

Parameters	H8BA	H6BA
Dipole and gradient of combined function bend (T, T/m)	0.529, 30.7	
Dipole and gradient of the first RB[a] (T, T/m)	0.248, 38.6	0.249, 44.8
Dipole and gradient of the second RB (T, T/m)	0.175, 57.1	0.225, 48.1
Quadrupoles B′ (T/m)	65.5–86.6	62.6–89.5
Sextupoles B″ (T/m^2)	1164–3156	1199–3626
Octupoles B‴ (T/m^3)		33 000

[a]For the two lattices, the first RB family is located in the high dispersion region, and the second one is in the middle region.

TABLE III. Comparison of emittance-related parameters of HMBA lattices with split bends.

Parameters	H8BA[a]	H9BA[b]	H6BA[c]	H6BA[d]
Energy (GeV)		3		
Number of cells	20	20	24	24
Cell horizontal tune	2.807	2.758	2.175	1.753
Designed/scaled natural emittance ε_x (pm rad)	74.5	80.0	136.2	259.2
J_x	1.91	2.00	1.58	1.78
Normalized emittance $\varepsilon_x \cdot J_x$ (pm rad)	142.3	160.0	215.2	461.4

[a]H8BA is designed in this paper.
[b]H9BA is scaled from the SSRL-X design, where the natural emittance is 63 pm rad with 3.5 GeV and 24 cells.
[c]H6BA is designed in this paper.
[d]H6BA is scaled from the design in Ref. [11], where the natural emittance is 38.4 pm rad with 6.0 GeV and 72 cells.

when observed in the straight section, although they are canceled when observed in the middle part of the arc section. Figure 8 shows the transverse phase space tori tracked at two locations. We see that the horizontal phase space tori is much distorted at the center of the straight section. Especially for the outermost tori, the horizontal position coordinate can be larger than 15 mm, which can result in particle loss on the physical aperture. However, when rf cavity and errors are included, the actual DA is reduced as shown in Fig. 7, and the phase space tori will also become smaller. For smaller tori, the distortion is much smaller as shown in Fig. 8. For the DAs with rf cavity (including the error case) in Fig. 7, a physical aperture with a radius of 11 mm was included in the tracking, and it was found that the tracked DAs remain the same if the physical aperture is not included. Besides, IDs installed in straight sections may disturb the nonlinear cancellation, while the

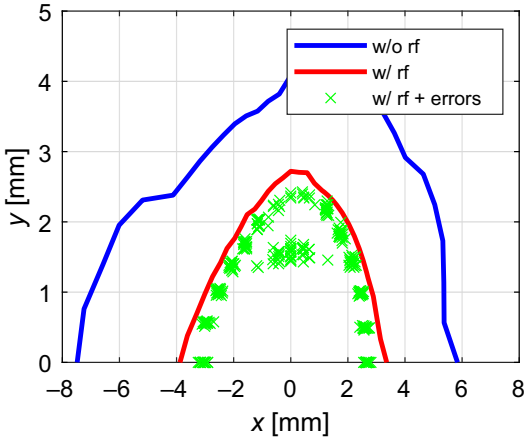

FIG. 7. On-momentum DA of the H8BA lattice, tracked at the center of the straight section with 1024 turns. The 4D DA shown in blue color was tracked without physical aperture, and the other two cases were tracked with physical aperture of radius 11 mm.

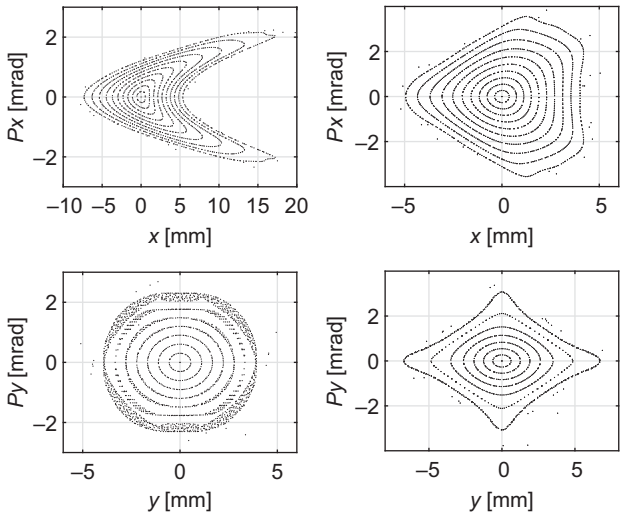

FIG. 8. Horizontal (top) and vertical (bottom) phase space tori of the H8BA lattice, tracked at the center of the straight section (left) and the center of the arc section (right) with 1024 turns.

low beta functions in straight sections are beneficial for reducing the tune shifts and beta-beat produced by IDs, and we can compensate for these changes. Here we will not further study the ID effect and compensation. Anyway, for this lattice, we can adopt the on-axis swap-out injection [30], which can allow a DA of only ~1 mm. Figure 9 shows the frequency map analysis of on-momentum DAs tracked at the center of the arc section for the perfect lattice and the lattice with a seed of errors. The error seed comes from the error settings above. It is seen that low diffusion rates dominate the DA of the perfect lattice and the DA with errors does not decrease much.

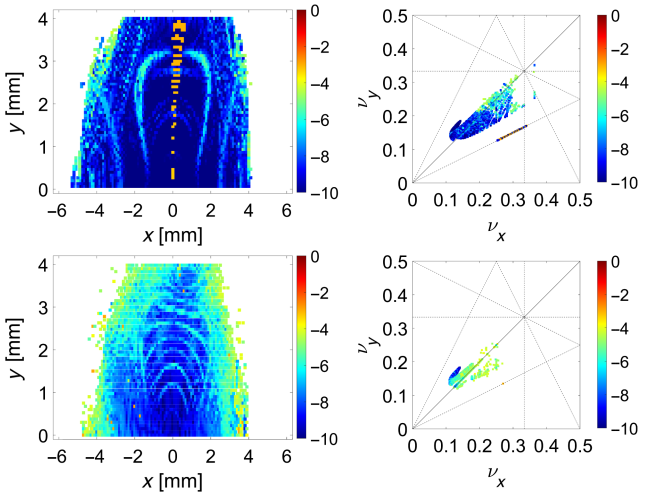

FIG. 9. Frequency map analysis of on-momentum DAs without errors (top) and with a seed of errors (bottom), tracked at the center of the arc section with 1024 turns. The color bar represents the diffusion rate.

B. H6BA lattice

To reflect the flexibility of the new lattice concept, an H6BA lattice is also designed, shown in Fig. 10, which removes the two central combined-function bends from the H8BA lattice. The natural emittance is 136.2 pm rad. The main storage ring parameters and the strengths of magnets (except LGBs) are also listed in Tables I and II, respectively. Recently, an H6BA lattice with split bends used and low beta in the straight was proposed [10,11] and adopted by PETRA IV [31], but the two central bend cells are constrained by $-I$ with transverse phase advances of (π, π). The horizontal tune of the H6BA lattice cell here is near 2.2, obviously larger than the value of about 1.75 for the H6BA lattice cell in Ref. [11], which is beneficial for reducing the emittance, as shown in the comparison made in Table III. In Table III, for the same energy and number of cells, the natural emittance of the H6BA lattice here is only about half that of the H6BA lattice in Ref. [11]. As said before, this can also reduce the damping times for an emittance goal so as to better suppress the IBS effect. It is interesting to note that the two central bends can also be seen as a split bend. If we regard the split bend as a single bend, then this H6BA lattice can be seen as a triple-bend achromat lattice [32].

Three sextupole families and one octupole family were employed in the nonlinear optimization of this H6BA lattice, where the chromaticities were also corrected to (2, 2). Figure 11 shows the horizontal DAs for a range of momentum deviations. The on-momentum horizontal DA is larger than 6 mm and reduces to about 4 mm with the rf cavity considered, and the dynamic momentum acceptance is large. The local momentum apertures (LMAs) are shown in Fig. 12. Based on the LMAs with errors, the average Touschek lifetime was calculated, which is about 5 h for a 10%-coupling beam with a bunch charge of 1 nC and with bunch lengthened by a factor of 4 using a harmonic cavity. If there is no bunch lengthening, the Touschek lifetime is

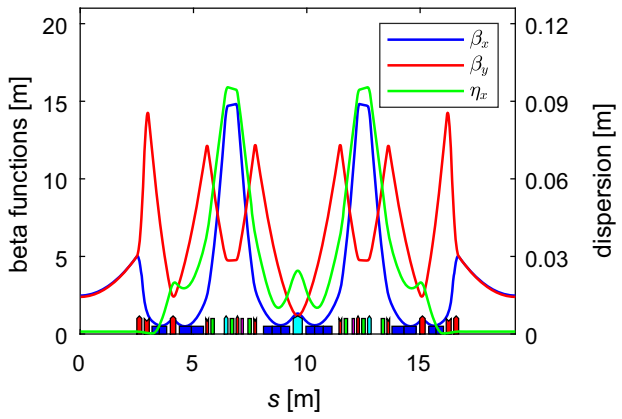

FIG. 10. Magnet layout and optical functions of the H6BA lattice cell. Octupoles are in pink, and the other magnets are as in Fig. 6.

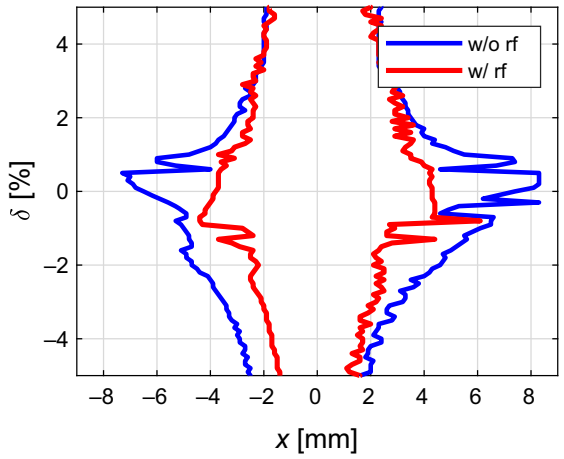

FIG. 11. Horizontal DAs of the H6BA lattice for relative momentum deviations of −5% to 5%, tracked at the center of the straight section with 1024 turns. The 4D DAs are shown in blue and the DAs tracked with the rf cavity are in red.

3.1 h for the perfect lattice and it is about 1.6 h for the error case. The reason that the lifetime decreases much in the error case is that the off-momentum DAs are obviously smaller than those of the perfect case.

The H6BA design has more straight sections than the H8BA, and we can place some DWs in straight sections to further reduce the emittance and also to reduce the damping times for suppressing IBS induced emittance increase. With four DWs employed, each with a length of 4.2 m, a peak field of 2.2 T, and a period of 105 mm, the natural emittance is reduced to 88.4 pm rad. And the damping times (H/V/L) are reduced to 8.3/10.6/6.1 ms with J_x of 1.27, smaller than that without DW. When including IBS, the horizontal emittance increases to 99.2 pm rad for the beam as in the

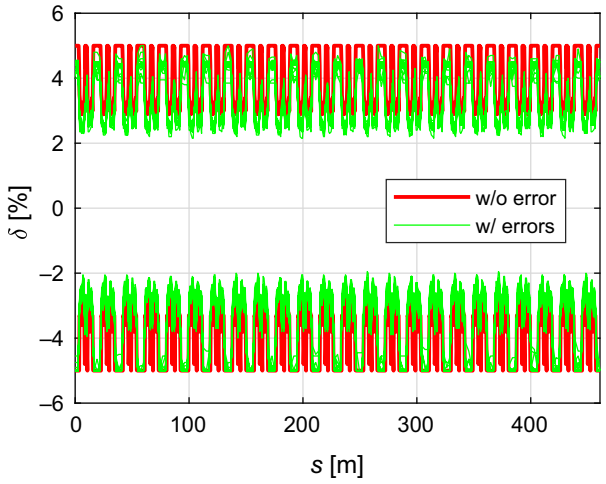

FIG. 12. LMAs of the H6BA lattice tracked along the ring with 3000 turns. In the tracking, rf cavity and physical aperture of radius 11 mm were considered, and the rf momentum acceptance was set to 5%.

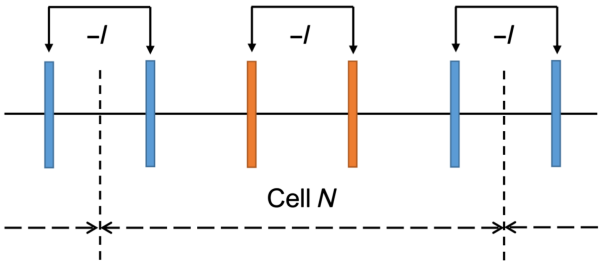

FIG. 13. Schematic of an MBA lattice with two pairs of $-I$ separated dispersion bumps. The dashed vertical lines indicate the centers of straight sections.

Touschek lifetime calculation with bunch lengthening. If a full-coupling beam is used, the horizontal emittance can be further reduced and the horizontal emittance increase due to IBS can also be better suppressed. Furthermore, in these two lattices, if the transverse gradient is introduced in split bends as in Refs. [10,11,16,31], their natural emittances can be further reduced.

IV. EXTENSION

The nonlinear cancellation scheme proposed above can be extended to produce other MBA lattices. If the emittances of DLSRs are further reduced, such as ∼10 pm rad emittance design for MAX IV future upgrade [33], the number of bends in an MBA lattice will increase. If conventional MBA lattices are used, like a 19BA lattice for MAX IV upgrade [33], the magnet strengths will be extremely strong and the magnet layout will be unusually compact. A possible solution to mitigate the magnet and space issue is to use an HMBA-like lattice with few dispersion bumps. If there is only one pair of bumps in an MBA lattice with many bends, like the ALS-U 9BA lattice [34] and the H10BA lattice [9], it is very hard to have good off-momentum nonlinear dynamics for a reasonable beam lifetime. Introducing another pair of bumps may improve the off-momentum nonlinear dynamics [35]. Figure 13 shows the schematic of an MBA lattice with two pairs of $-I$ separated bumps. The two pairs of bumps are noninterleaved: the inner pair is inside the cell and the outer pair is the same as the scheme proposed in this paper. This noninterleaved layout is good for improving nonlinear dynamic performance.

Besides, due to that the inner part of the arc section in the new HMBA lattice is free, it can be easily extended to a combined lattice, HmBA-HnBA lattice ($m \neq n$), without affecting the nonlinear cancellation.

V. CONCLUSION

In this paper, we studied a new HMBA lattice concept to make the main arc section free of the phase advance constraint so as to increase the flexibility of the lattice. In the concept, $-I$ transformation for sextupole cancellation is moved to both sides of the lattice cell. To increase the phase advances for satisfying the $-I$, split bends are used as matching bends, which also reduce the emittance, and beta functions in the straight section are lowered, which is also good for enhancing ID brightness. The bend unit cells of the new HMBA lattice can have stronger focusing than those of the typical HMBA lattice, which is beneficial for reducing the emittance and also for suppressing the IBS effect for a given emittance goal. The DA of the new lattice is relatively large, but the phase space tori are distorted in the straight section due to that the nonlinear cancellation made across the straight section. This cancellation scheme can also be extended to produce other MBA lattices for DLSRs.

ACKNOWLEDGMENTS

This work was supported by the National Key Research and Development Program of China under Grant No. 2016YFA0402000 and the National Natural Science Foundation of China under Grants No. 11875259 and No. 12205299.

[1] James B. Murphy, Synchrotron light source data book, AIP Conf. Proc. **249**, 1939 (1992).
[2] D. Einfeld, M. Plesko, and J. Schaper, First multi-bend achromat lattice consideration, J. Synchrotron Radiat. **21**, 856 (2014).
[3] L. Farvacque, N. Carmignani, J. Chavanne, A. Franchi, P. Raimondi *et al.*, A low-emittance lattice for the ESRF. in *Proceedings of the 4th International Particle Accelerator Conference, IPAC-2013, Shanghai, China* (JACoW, CERN, Geneva, Switzerland), pp. 79–81.
[4] P. Raimondi, N. Carmignani, L. R. Carver, J. Chavanne, L. Farvacque, G. Le Bec, D. Martin, S. M. Liuzzo, T. Perron, and S. White, Commissioning of the hybrid multibend achromat lattice at the European Synchrotron Radiation Facility, Phys. Rev. Accel. Beams **24**, 110701 (2021).
[5] M. Borland, R. Lindberg, T. Berenc, V. Sajaev, and Y. Sun, Lower emittance lattice for the Advanced Photon Source Upgrade using reverse bending magnets, in *Proceedings of North American Particle Accelerator Conference, NAPAC'16, Chicago, IL* (JACoW, Geneva, Switzerland, 2016), pp. 877–880.
[6] A. Streun, The anti-bend cell for ultralow emittance storage ring lattices, Nucl. Instrum. Methods Phys. Res., Sect. A **737**, 148 (2014).
[7] A. Alekou, R. Bartolini, T. Pulampong, N. Carmignani, and P. Raimondi, Study of a double triple bend achromat (DTBA) lattice for a 3 GeV light source, in *Proceedings of IPAC'16, Busan, Korea* (JACoW, Geneva, Switzerland, 2016), pp. 2940–2942.
[8] Z. Bai, G. Feng, T. He, W. Li, W. Li *et al.*, A modified hybrid 6BA lattice for the HALF storage ring, in *Proceedings of 12th International Particle Accelerator Conference, IPAC'21, Campinas, SP, Brazil* (JACoW, Geneva, Switzerland, 2021), pp. 407–409.

[9] P. Yang, Z. Bai, T. Zhang, D. Xu, and L. Wang, Design of a hybrid ten-bend-achromat lattice for a diffraction-limited storage ring light source, Nucl. Instrum. Methods Phys. Res., Sect. A **943**, 162506 (2019).

[10] P. Raimondi, Beyond EBS, in *ESRF Webinars* (ESRF, Grenoble, 2021), https://www.youtube.com/watch?v=unvO4QVfN5M.

[11] Pantaleo Raimondi and Simone Maria Liuzzo, Toward a diffraction limited light source, Phys. Rev. Accel. Beams **26**, 021601 (2023).

[12] A. Streun, T. Garvey, L. Rivkin, V. Schlott, T. Schmidt, P. Willmott, and A. Wrulich, SLS-2–the upgrade of the Swiss Light Source, J. Synchrotron Radiat. **25**, 631 (2018).

[13] P. Yang, W. Li, Z. Ren, Z. Bai, and L. Wang, Design of a diffraction-limited storage ring lattice using longitudinal gradient bends and reverse bends, Nucl. Instrum. Methods Phys. Res., Sect. A **990**, 164968 (2021).

[14] G Baranov, A Bogomyagkov, I Morozov, S Sinyatkin, and E Levichev, Lattice optimization of a fourth-generation synchrotron radiation light source in Novosibirsk, Phys. Rev. Accel. Beams **24**, 120704 (2021).

[15] Z. H. Bai, Lattice design progress of the HALF storage ring, in *3rd Workshop on Low Emittance Lattice Design—LEL 2022* (ALBA, Barcelona, Spain, 2022), https://indico.cells.es/event/1072/contributions/1787/.

[16] J. Kim, X. Huang, P. Raimondi, J. A. Safranek, M. Song *et al.*, A hybrid multi-bend achromat lattice design for SSRL-X, in *Proceedings of 13th International Particle Accelerator Conference, IPAC'22, Bangkok, Thailand* (JACoW, Geneva, Switzerland, 2022), pp. 207–209.

[17] G. S. Jang, S. Shin, M. Yoon, J. Ko, Y. D. Yoon, J. Lee, and B.-H. Oh, Low emittance lattice design for Korea-4GSR, Nucl. Instrum. Methods Phys. Res., Sect. A **1034**, 166779 (2022).

[18] A. Bogomyagkov, E. Levichev, and P. Piminov, Low emittance lattice cell with large dynamic aperture, arXiv:1405.7501.

[19] A. Loulergue, P. Alexandre, P. Brunelle, L. Hoummi, O. Marcouillé *et al.*, Baseline lattice for the Upgrade of SOLEIL, in *Proceedings of International Particle Accelerator Conference, IPAC'18, Vancouver, BC, Canada, 2018* (JACoW Publishing, Geneva, Switzerland, 2018), pp. 4726–4729.

[20] L. C. Teng, Minimizing the emittance in designing the lattice of an electron storage ring, Fermi National Accelerator Laboratory Technical Report No. TM-1269, 1984.

[21] Y. Yuan, H. Xu, and B. Wang, An improved NSGA-III procedure for evolutionary many-objective optimization, in *Proceedings of GECCO '14, New York, NY* (Association for Computing Machinery, 2014), pp. 661–668.

[22] S. Y. Lee and L. Teng, Theoretical minimum emittance lattice for an electron storage ring, in *Proceedings of the Conference Record of the 1991 IEEE Particle Accelerator Conference, San Francisco, CA* (IEEE, New York, NY, 1991), Vol. 5, pp. 2679–2681.

[23] Jianhao Xu, Penghui Yang, Gangwen Liu, Zhenghe Bai, and Weimin Li, Constraint handling in constrained optimization of a storage ring multi-bend-achromat lattice, Nucl. Instrum. Methods Phys. Res., Sect. A **988**, 164890 (2021).

[24] Ryan R. Lindberg and Kwang-Je Kim, Compact representations of partially coherent undulator radiation suitable for wave propagation, Phys. Rev. ST Accel. Beams **18**, 090702 (2015).

[25] Ryutaro Nagaoka and Albin F. Wrulich, Emittance minimisation with longitudinal dipole field variation, Nucl. Instrum. Methods Phys. Res., Sect. A **575**, 292 (2007).

[26] Andreas Streun and Albin Wrulich, Compact low emittance light sources based on longitudinal gradient bending magnets, Nucl. Instrum. Methods Phys. Res., Sect. A **770**, 98 (2015).

[27] Andreas Streun. OPA web site, https://ados.web.psi.ch/opa/.

[28] M. Borland, ELEGANT: A flexible SDDS-compliant code for accelerator simulation, Advanced Photon Source Report No. LS-287, 2000, https://publications.anl.gov/anlpubs/2000/08/36940.pdf.

[29] J. Bengtsson, The sextupole scheme for the Swiss Light Source (SLS): An analytic approach, SLS Internal Report No. Note 9/97, 1997, https://ados.web.psi.ch/slsnotes/sls0997.pdf.

[30] L. Emery and M. Borland, Possible long-term improvements to the Advanced Photon Source, in *Proceedings of the 20th Particle Accelerator Conference, PAC-2003, Portland, OR* (IEEE, New York, 2003), pp. 256–258.

[31] I. V. Agapov, S. Antipov, R. Bartolini, R. Brinkmann, Y. C. Chae *et al.*, PETRA IV storage ring design, in *Proceedings of 13th International Particle Accelerator Conference, IPAC'22, Bangkok, Thailand* (JACoW, Geneva, Switzerland, 2022).

[32] A. Jackson, A comparison of the Chasman-Green and triple-bend achromat lattices, Part. Accel. **22**, 111 (1987), https://cds.cern.ch/record/167601/files/p111.pdf.

[33] Pedro Fernandes Tavares, Johan Bengtsson, and Åke Andersson, Future development plans for the MAX IV light source: Pushing further towards higher brightness and coherence, J. Electron Spectrosc. Relat. Phenom. **224**, 8 (2018).

[34] Changchun Sun, H. Nishimura, D. Robin, F. Sannibale, C. Steier *et al.*, Design of the ALS-U storage ring lattice, in *Proceedings of 8th International Particle Accelerator Conference, IPAC'17, Copenhagen, Denmark* (JACoW, Geneva, Switzerland, 2017), pp. 2827–2829.

[35] Zhenghe Bai, Wei Li, Gangwen Liu, Derong Xu, Tong Zhang, and Lin Wang, Study of seven-bend achromat lattices with interleaved dispersion bumps for HALS, in *Proceedings of 10th International Particle Accelerator Conference, IPAC'19, Melbourne, Australia* (JACoW, Geneva, Switzerland, 2019), pp. 1495–1497.